United States Department of Interior
Geological Survey

PETROGRAPHIC STUDY OF FLUID INCLUSIONS IN SALT CORE SAMPLES FROM ASSE MINE, FEDERAL REPUBLIC OF GERMANY

by Edwin Roedder and H.E. Belkin

Open File Report 81-1128

Interagency Agreement DE-AI97-79ET44611

Petrographic study of fluid inclusions in salt core samples from Asse mine, Federal Republic of Germany,

by Edwin Roedder and H.E. Belkin

INTRODUCTION

Under Department of Energy/U.S. Geological Survey Interagency Agreement DE-AI97-79ET44611, we were asked by M.W. Anthony of the Office of Nuclear Waste Isolation, on 5 March, 1981, to examine samples of salt cores from the brine migration test area in the Asse mine, Federal Republic of Germany. The Asse mine is the location of a planned heater test to determine brine migration characteristics in salt in connection with atomic waste disposal in salt. The 12 samples of core were shipped by ONWI to Oak Ridge National Laboratory for splitting, and our splits were received on 1 April, 1981. It was immediately obvious on examining the samples as received that they would not be suitable for any quantitative determinations of water content. Due to the coring procedures used, an unknown but probably large percentage of the water originally present was almost certainly lost, as detailed in a letter from Roedder to M.W. Anthony of 3 April, 1981.

One of the most important parameters in any brine migration test design is the source term -- the nature and amount of water present in situ in the salt in the vicinity of the test chamber. The various preliminary calculations for the test plan for Asse are all based on the assumption of the presence of 0.05 wt.% H_2O, of which little, if any, is assumed to be present as liquid inclusions. This assumption is based,

in turn, on a report by Jockwer (1979), but in several other papers on Asse salt, Jockwer (1980; and personal communication) shows thermogravimetric analysis curves in which approximately 1/2 of the water loss below 240°C occurs at ~100°C. Jockwer calls this "crystal boundary surface water" but its behavior is exactly as would be expected for liquid inclusion water that has been exposed during his sample preparation procedure (which involved ball milling to < ~1mm).

It was hoped that petrographic examination of these core samples, in spite of their deficiencies, would help to clarify the question of the nature, if not the amount, of water present in the Asse salt.

NATURE OF THE SAMPLES AS RECEIVED

The drill core axis was presumed to have been strongly inclined to any expected compositional banding in the salt, but some of the core splitting was done perpendicular to the core axis, rather than parallel to it. The position of the cut surfaces relative to visible color differences may well result in significant differences between the several splits of any given core sample. For the record, the size and nature of the samples received are listed in Table 1.

WEIGHT % INSOLUBLE RESIDUE

Some of the samples appeared to contain appreciable quantities of minerals other than halite, so a portion (averaging 14g) of each was leached with water at room temperature, with frequent decanting, for 8 days. This dissolved all halite, kieserite, carnallite, and other readily water-soluble minerals but left the insoluble and very slightly

Table 1-Sample List

No.	Shape	Length* (cm)	Wt.%** Insol.	Nature of salt and relationship of sample surfaces
8R	Hemicylinder	5	12.9	Uniform gray; one end broken; other end a sawcut perpendicular to core axis.
11R	"	2	0.29	Uniform white; one end broken, other end a sawcut perpendicular to core axis.
14R	"	3	14.1	Same as above.
17R	"	5	23.7	White on one end (broken); other end gray and a sawcut perpendicular to core axis.
20R	"	4	16.7	Dark band through middle, perpendicular to core axis. One end broken, other end a sawcut perpendicular to core axis.
24R	Cylinder	1.5	0.02	Uniform white; both ends broken surfaces.
27R	"	1.5	0.34	Uniform white; one end broken; other end a sawcut perpendicular to core axis. An additional sawcut along a diameter (i.e., parallel to core axis) cuts the sample into two hemicylinders.
30R	Hemicylinder	3.5	11.4	Uniform white; both ends broken surfaces.
33R	"	4	8.3	Uniform white; one end broken; other end a sawcut perpendicular to core axis.
35R	"	5	6.8	Uniform white except for olive green stains on outer core surfaces; both ends broken surfaces.
38R	"	3.5	5.8	Uniform white; one end broken; other end a sawcut perpendicular to core axis.
41R	"	3.5	8.6	Same as above.
			Avg. 9.1	

* Along core axis
** See text

soluble grains (mainly anhydrite). The precision of this test was not determined, but the visible heterogeneity of the salt and the necessarily small sample size made it obvious that the precision would be poor. The amount of insolubles found ranged from 0.02 to 23.7 wt % (Table 1), and averaged surprisingly high, 9.1 wt %.

PREPARATION OF DOUBLY POLISHED PLATES AT USGS

The largest flat surface on each sample was ground and polished. This surface was either parallel or perpendicular to the core axis, as listed in Table 1. This polished surface was cemented to a glass slide with room-temperature-curing epoxy resin and a saw cut made, with a slow-speed diamond wafering saw and saturated brine as lubricant, leaving a plate approximately 5mm thick on the glass. This sawn surface was then polished also. All sawing, grinding, and polishing was done with care to avoid surface heating and cracking. Final polishing was done by hand with 0.3μm Al_2O_3 powder and saturated brine on a sequence of drier and drier papers.

OBSERVATIONS AT LOW MAGNIFICATION

Overall cracking

Most doubly polished plates of polycrystalline salt have grain boundaries outlined by planes of minute solid inclusions (clay or other minerals), fluid inclusions (gas or liquid), or cracks. However, all 12 plates of the Asse salt samples showed extensive intergranular cracking, to the extent that little of the area of salt was transparent in the 5-mm thick doubly polished plates. This cracking outlines all grain boundaries and many individual salt crystals have cleavage cracks, so that only a few crack-free 1-cm crystals were found. Most areas on the plate have cracks at a spacing of only a few millimeters. Three samples, 8R, 11R, & 17R,

illustrate the range of cracking found (Figs 1-3). In Fig. 1 the cracks outlining grain boundaries reveal a strong fabric (elongation of the salt crystals, presumably from flowage) inclined ~60° to the core axis. In Fig. 2 (necessarily cut perpendicular to the core axis), no such fabric is seen. In Fig. 3, two large, unfractured salt crystals are seen to be embedded in a more intensely cracked matrix which shows some degree of orientation similar to that in Fig. 1. (These two large crystals have some special features noted below).

Cracking at core surface

The dry coring operation used to obtain these samples resulted in extensive damage to the surface of the cores. This outside, cylindrical surface is opaque white in hand specimen, and in the plates this whiteness is seen to be due to very closedly spaced fractures throughout a zone that generally is at least 3mm in thickness. It is most obvious in Fig. 2, where almost no crystal of salt within 4mm of the core surface is transparent. This 4-mm zone represents 31 volume percent of this core. Visibly cracked salt in this sample extends in at least 10mm from the core surface, and includes over 60% of the entire core.

MICROSCOPY

Intracrystalline inclusions

Only a relatively few grains in these samples contain fluid inclusions; the bulk of the grains contain essentially no visible inclusions. Those few grains that contain them, however, frequently contain many inclusions, of several types, as detailed below. No recognizable pattern was seen in the distribution of the various types of inclusions in the 12 samples; their distribution is so erratic that many more plates would have to be

cut to verify any such relationship.

"Primary" inclusions. Most inclusions in most salt samples cannot be considered "primary" in the normal sense, i.e., trapped during the original crystal growth, since most salt has been recrystallized after its original formation. Only one example of valid primary inclusions was found, in which the inclusion array was definitely related to the original cubic crystal growth pattern (Fig. 4). Whether this crystallization occurred in Permian seas or during some subsequent recrystallization is unknown.

Several other salt crystals were found that contained a similar concentration of relatively large inclusions, although without any regular crystallographically controlled array. Fig. 5 shows one such inclusion-rich grain, and Fig. 6 is a closeup of some of these inclusions. Optical measurements of the inclusions in some of these grains showed them to have as much as 2.4 wt. % H_2O as brine. Most such inclusions contain a group of birefringent crystals in brine, plus a small bubble (Fig. 6), but some have little or no solid phase (Fig. 7). Many such inclusion-rich salt grains have at least a portion of the same crystal that is free of inclusions (e.g., Fig. 8), and hence might possibly be remnants from partial recrystallization of originally zoned crystals such as Fig. 4.

Another type of "primary" inclusions is shown in Figs. 9 & 10. Scattered throughout the salt crystals in these samples are crystals of various other evaporite minerals, mainly anhydrite, carnallite, and kieserite (Jockwer, 1980). Some of the smaller grains of such minerals are found along the grain boundaries between halite crystals, but many occur as solid inclusions completely enclosed within halite single crystals. The interface between such crystals and the enclosing halite is frequently decorated with small (1-10μm) dark inclusions of high

pressure gas (see below). Such high pressure gas inclusions are commonly observed in domal salt and are probably responsible for some of the large spontaneous and disastrous mine "blowouts" of thousands of tons of salt in Louisiana salt domes and elsewhere (Roedder & Belkin, 1979, figs. 11-14, 23-24; Roedder, 1972, p.43). Presumably the gas inclusions formed on the interface since it represents the lowest energy configuration. These inclusions are "primary" only insofar as they were presumably formed during the diagenetic or low-grade metamorphic recrystallization that yielded the present fabric.

The last type of "primary" inclusion to be described occurs in large numbers and what appears to be high concentrations, but only in a few halite grains. The largest and best example of such grains is seen in Fig. 3. Several such inclusion-rich crystals are larger than the inclusion-free host salt, thus suggesting the strange conclusion that during flowage of the host salt these inclusion-rich grains were more resistant to deformation. At first glance, the distribution of inclusions seems to be relatively uniform throughout the grains, right up to the boundary where they abut other inclusion-free grains (Fig. 11). In detail, however, it is not uniform. Thus the single-crystal grain shown in Fig. 3 has a slight but real banding, and when viewed at higher magnification (Fig. 13), it is seen to have occasional larger inclusions, along with the large numbers of small ones. Other grains, e.g. Fig. 12, although uniform in distribution at low magnification, show a cellular structure at higher magnification, with most inclusions lying on a series of otherwise invisible three-dimensional "walls," outlining inclusion-free cells; the entire mass, however, is now a single crystal of salt, as revealed by the occasional cleavage fractures across such crystals. Some suggestion

of this cellular structure is also apparent in Fig. 13.

The amount of water in the inclusions in a grain such as seen in Fig. 13 is far less than the appearance would suggest. Two independent optical estimates of the volume of inclusions present in a visually representative volume of the crystal shown in Fig. 13 yielded values of only 0.015 and 0.04 weight percent H_2O.

The inclusions in these samples are practically all multiphase: liquid, several to many birefringent prismatic crystals, and, in some inclusions, a vapor bubble. Many of these inclusions are essentially masses of crystals with liquid in the interstices (Fig. 14). All gradations exist between amoeboid masses of wet crystals (Fig. 14) through globular shapes (Figs. 14 & 15) to more nearly cubic, negative crystal shapes (Figs. 16 & 17). Many of the amoeboid inclusions are surrounded by a halo of tiny birefringent cyrstals, each with adhering liquid inclusions on each side (Fig. 14), as though there had originally been a more diffuse, amoeboid inclusion, most of which has coalesced to the wet crystal masses we see now. Negative crystal shapes are only seen in inclusions with a high liquid/solid ratio.

Secondary inclusions - Secondary inclusions occur in healed fracture planes, so their secondary origin is reasonably obvious, but the problem of when they were trapped is not so obvious. A few large secondary inclusions were found in the fractured white zone at the edge of some of the cores (e.g. Fig. 18); these are presumed to result from the trapping of the saturated brine (used in the sawing and polishing) in the fractured salt.

Other planes of secondary gas and/or liquid inclusions that occur at some distance from the core edge, may be from fracturing in nature,

or they may be artifacts from sample preparation. Those planes shown in Figs. 21-23 are probably indigenous and not artifacts, since similar but less photogenic planes of secondary inclusions were also seen in cleavage fragments from these samples that were never exposed to liquid in the laboratory. All such planes that were studied on the freezing stage (see below) were found to be indigenous.

At least some secondary inclusion planes must be indigenous, as they contain not just brine, but droplets of an immiscible fluid of higher index of refraction than the brine (presumably petroleum) and no petroleum was used in the sample preparation. Figs. 19 & 20 illustrate one such plane. Oily films also were seen to collect on the surface when some of the Asse samples were dissolved in water.

Intercrystalline inclusions and the grain boundaries

The grain boundaries between salt crystals in rock salt are seldom simple sharp, clean contacts between two salt grains. In most rock salt, the grain boundaries are the site of small grains of other accessory minerals, fluid inclusions, miscellaneous unidentified opaque particles, and frequently they are also cracks. Asse salt is no exception. When these samples are viewed both in reflected and transmitted light, several interesting features are seen. In transmitted light, the grain boundaries are opaque (Figs. 1-3), except when they are tipped to become more or less perpendicular to the line of sight. This opacity arises from total reflection, and occurs only when there is a contrast in index of refraction on the two sides of the interface. Two salt crystals in close contact will not yield total reflection, since they have the same index (1.545). But if there is a film between the two crystals that has a different index (e.g., a film of brine of index ~1.3, or of air of index 1.0),

total reflection can occur. The angle (between the perpendicular to the interface and the line of sight) above which total reflection will occur varies inversely with the difference in index across the interface. The fact that practically all grain boundaries in the Asse salt plates exhibit total reflection means that they all have films of a different index, probably of air (i.e., cracks). In order to cause total reflection, such films or cracks must have a thickness at least on the order of the wavelength of the light used (~0.5 μm), and so they are not very visible in light reflected from a polished surface. Figs. 24-26 show three grains of salt, A, B, & C in a doubly polished plate. Both intercrystalline boundaries are almost completely opaque in transmitted light, but in reflected light, that between A and B shows only a faint "hairline" crack (arrow), whereas that between B and C is much more pronounced. Both are "decorated" with inclusions (black spots in Fig. 25). Grain C has two parallel intragranular cleavage cracks that are also decorated with inclusions. Figs. 24 & 25 were taken at the same time. After additional futile attempts to improve the polish, the sample was stored in a desiccator for several days and rephotographed in special reflected light illumination to reveal the surface incrustations formed from fluid creeping out of the fractures (Fig. 26).

Most of the grain boundaries have a mottled appearance in transmitted light, with black spots (e.g. Fig. 27). When such a sample is rotated so that the sloping grain boundary becomes more nearly perpendicular to the line of sight, these black spots suddenly become transparent, since they are mostly not from opaque materials, but merely from total reflection of the more steeply inclined portions of an irregular, bumpy interface between two crystals. The same area of Fig. 27 is seen in reflected

light in Fig. 28, where several inclusions are seen along the almost invisible hairline crack between the two grains. After a new repolishing, Fig. 29 shows no inclusions and only a faint hairline crack is visible (arrow); this illustrates an important caveat about such work with salt: hairline cracks can be made to appear wider, or to almost disappear, by the polishing technique used.

Almost all grain boundaries in the Asse salt are decorated with at least some inclusions (mostly now air-filled, due to the interconnecting cracks) and many of the accessory mineral grains present occur there as well (e.g., Fig. 30). The significance of this is that if these are hydrous phases, the water they may evolve on decomposition is immediately available for migration on a grain boundary.

The presence of hairline cracks between many grains raises a question as to what holds these core samples together. (The samples were considered to be too brittle to be used for rock mechanic laboratory analysis.) Fig. 31 shows that some of the grain boundaries are rather complex and crenulate; such crenulations can hold the sample together even though there is a crack along the boundary.

Evidence of leakage of fluid inclusions

Although there is some evidence for a fluid gain via some new secondary inclusions introduced into these samples during sample preparation, as shown above, we are reasonably sure that the fluid loss by emptying of indigenous fluid inclusions via cracks introduced in the coring operation will be quantitatively much larger. A number of the larger liquid-filled inclusions in these samples have been partly or completely drained through visible fractures assumed to have been introduced by the coring. An example is given in Figs. 32-33. Here a fracture has emptied some of a

group of large inclusions, and rehealing of the fracture has trapped a new plane of secondary gas and liquid inclusions.

Freezing stage results

Several inclusions were studied on the freezing stage in order to determine the salinity of the inclusion fluids from the depression of the freezing point (Roedder, 1962). A rather large (~100 μm) inclusion in sample 14R, consisting of a wet mass of birefringent crystals (~90% solids), was found to have a sufficiently large area of clear liquid to test. After it froze (at -115°C), visible recrystallization occurred at -80°C, suggesting a trace of liquid was present, and visible liquid was seen at -49.5°C. Ten other similar nearby inclusions showed similar results. Major melting occurred at ~-5.6°C, and the last recognizable ice melted at -3.3°C.

A plane of ~30 secondary all liquid or liquid plus vapor inclusions in this same sample showed first visible melting at ~-52°C and the last recognizable ice melted at -5.4 to -3.2°C (verified with a second run).

Still another group of secondary liquid or liquid plus vapor inclusions in this sample had first visible melting at -50.6°C and last melting of ice at -5.6 to 0.0°C. A group of 8 secondary inclusions in a plane in sample 30R yielded similar results: first visible melting at -46.7 to -48.2 and last ice melting at -1.2 to -1.0°C.

These results prove that the inclusions studied were indigenous and not from laboratory preparation, since the very low temperatures of first appearance of liquid found can only be the result of $CaCl_2$ in the solutions. No other constituent of natural fluids can result in such low eutectic melting. The widely variable temperatures of melting of the

last ice indicates that different groups of inclusions contain different composition fluids, presumably trapped at different times.

Solution release of gas pressure within inclusions

Normally the crushing stage (Roedder, 1970) is used to reveal the presence of gases under presure in fluid inclusions. However, as salt is soluble in water, a much easier technique is to simply watch the advancing solution front as it approaches the inclusion of interest. Just as the crushing stage test, it is extremely sensitive to the presence of gases under pressure. Typical behavior of inclusions in Asse salt is shown in Figs. 34-36. From a series of such tests, it is evident that small high pressure gas inclusions are commonly present on the interface between salt and most (~70%) of the enclosed crystals of other phases, as well as on some salt grain boundaries. The nature of the gas is not known at present, but it is not readily soluble in water, as the bubbles expanded out into water when the solution front contacted the inclusions. These gases may also be present as invisible films around some grains, rather than as discrete inclusions. Most inclusions of liquid plus crystals (such as Fig. 14) contain at least some gas and develop a bubble when the pressure is released. About 95% of all flat one or two-phase secondary inclusions formed bubbles on solution release, and all equant 2-phase inclusions (such as Fig. 7) showed 2- to 15-fold expansion of the bubble on release. The average was about 10-fold, and hence suggests ~10 atm pressure in these bubbles. The volume expansion of the small dark inclusions on interfaces (such as Figs. 34 & 35) was considerably more than 10-fold, suggesting very high pressures, but the pressure cannot be readily quantized since the volume of the tiny, irregular inclusions cannot

be measured accurately. This gas may be under hundreds of atmosphere pressure. No bubble that was visible before the solution front reached the inclusion was seen to collapse when the solution front broke in, so all contain noncondensable gas and none are merely from shrinkage on cooling to surface temperature. A few samples showed a slow expansion of the bubble ~2-4 seconds) suggesting that volatilization of a liquified gas (presumably organic) was involved.

SUMMARY

A series of 12 core samples from the Asse salt mine in F.R.G. have been studied to determine the amount and nature of fluid present as fluid inclusions. The samples as received were badly fractured due to the coring procedure used, and hence were completely unsuited for quantitative analysis of the water present, but some qualitative petrographic studies could be made. The salt was found to be relatively impure, as these samples contained an average of 9% by weight of insoluble residues, mainly anhydrite.

These samples contain water in at least three forms: intracrystalline (in part primary) fluid inclusions, intercrystalline (grain boundary) fluid inclusions, and hydrous minerals. Quantitative estimates are not possible due to the nature of the samples, but intracrystalline water may be larger than intercrystalline water. Practically all intercrystalline water and much of the intracrystalline water has been lost through cracks probably introduced during coring. Most of the grain boundaries are now hairline cracks from which fluid can be seen to ooze out over a period of a few days, and most hydrous accessory mineral grains lie along such grain boundaries. Some features of the very erratic distribution of the intracrystalline inclusions raise interesting and at present unanswered

questions concerning their genesis and the geological history of these salt deposits.

The fluid in these fluid inclusions is not simply a saturated NaCl brine, but a bittern that must contain very significant amounts of $CaCl_2$, plus gases of undetermined composition under relatively high pressure. The gas-rich inclusions could contribute to decrepitation of the walls during heating tests, and expansion of this gas might also help to push intergranular liquid to regions of lower pressure.

If valid data on the water content of the salt beds at the specific test site at Asse are to be obtained to use in calculations of the potential flow to be anticipated during the test, and to use as the source term in various mathematical models of brine migration after the test, more appropriate samples are required.

REFERENCES

Jockwer, N., 1979, Investigation on the migration and release of water within rock-salt in Waste Isolation Performance Assessment and In-situ Testing, Proc. U.S./F.R.G. Bilateral Workshop, Berlin, Oct. 1-5, 1979, p. 392-396.

Jockwer, N., 1980, Laboratory investigations on the water content within the rock-salt and its behavior in a temperature field of disposed high level waste (abst.): Materials Research Soc., Annual Meeting Program, Symposium D, p. D52.

Roedder, E., 1962, Studies of inclusions I: Low-temperature application of a dual-purpose freezing and heating stage: Econ. Geology, v. 57, p. 1045-1061.

Roedder, E., 1970, Application of an improved crushing microscope stage to studies of the gases in fluid inclusions: Schweiz. Mineral. Petrog. Mitteil., v. 50, p. 41-58.

Roedder, E., 1972, Composition of fluid inclusions, chapt. JJ. in: Data of Geochemistry, Michael Fleischer, ed., U.S. Geological Survey Prof. Paper 440JJ, 164 pp.

Roedder, E., and Belkin, H. E., 1979, Fluid inclusions in salt from the Rayburn and Vacherie domes, Louisiana: U.S. Geological Survey Open-File Report no. 79-1675; 25 pp.

Figs. 1-3 Double-polished plates (~5mm thick) of samples 8R, 11R, and 17R, in transmitted light (left) and in diffuse incident light, against a dark background (right). Scale bars 1 cm.

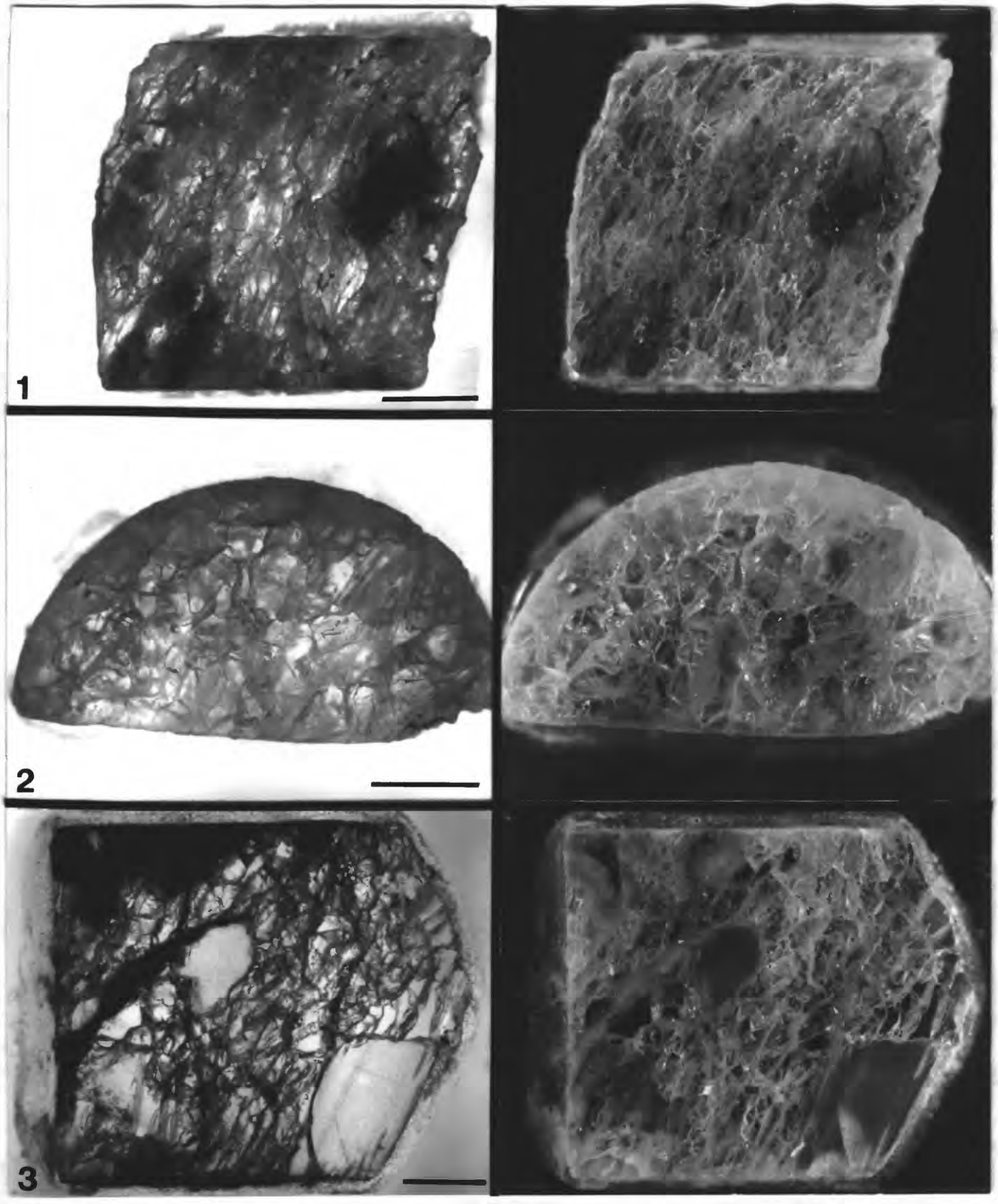
1
2
3

Fig. 4 Zoned cubic salt crystal with two zones of primary inclusions outlining the core and the rim of the crystal. Sample 38R. Scale bar 500 µm.

Fig. 5 Inclusion-rich salt crystal, sample 35R. Scale bar 1000 µm.

Fig. 6 Close-up of upper right part of Fig. 5, showing crystals in liquid inclusions. Note the (empty) inclusions outlining the cleavage boundary to right. Scale bar 100 µm.

Fig. 7 Close-up of another inclusion-rich crystal, showing vapor bubbles and a very few solid crystals in brine inclusions, from sample 24R. Scale bar 100 µm.

Fig. 8 Inclusion-rich crystal from sample 35R, in which part of same grain is completely free of inclusions, presumably due to recrystallization. Scale bar 100 µm.

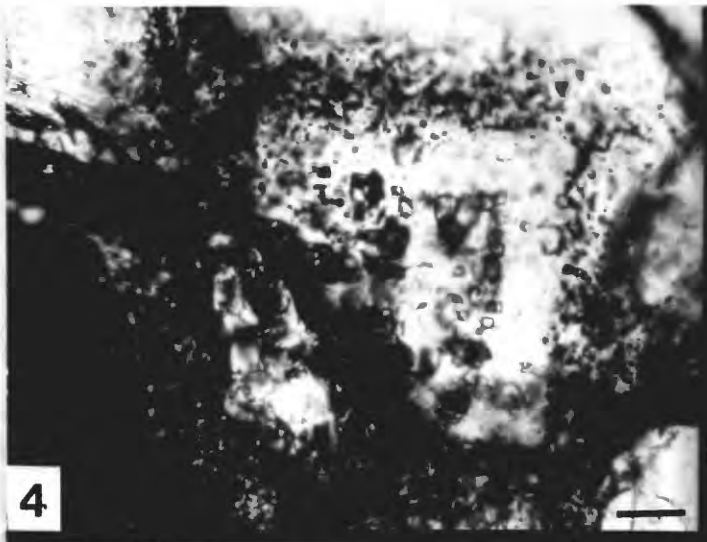
4

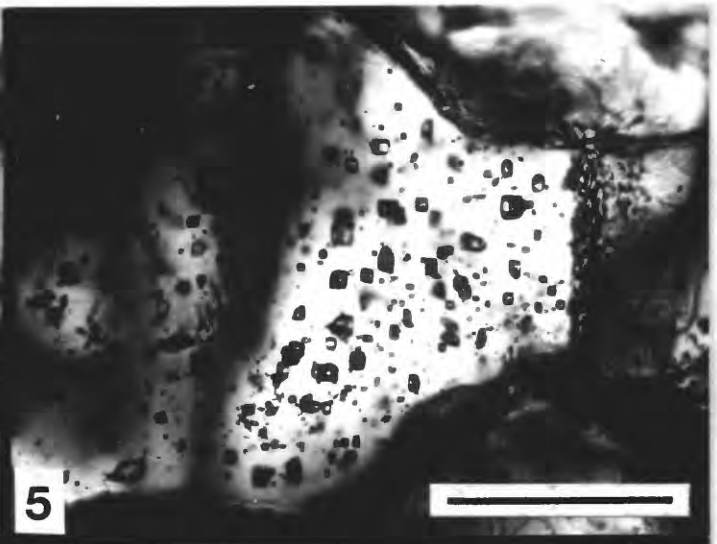
5

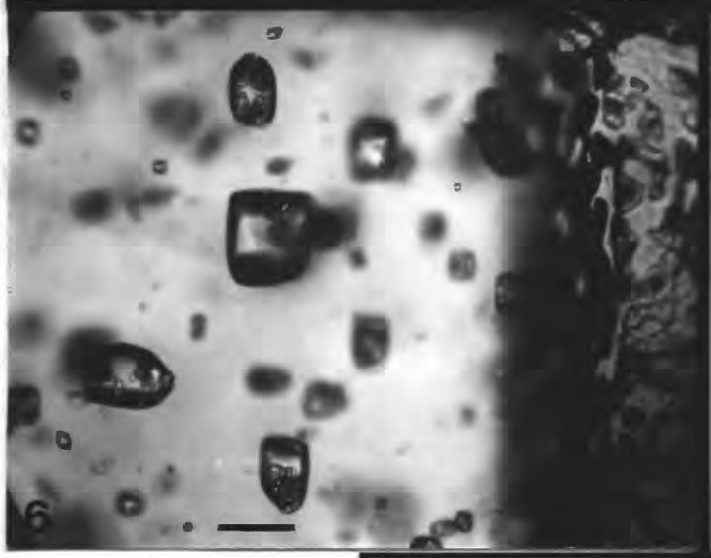
6

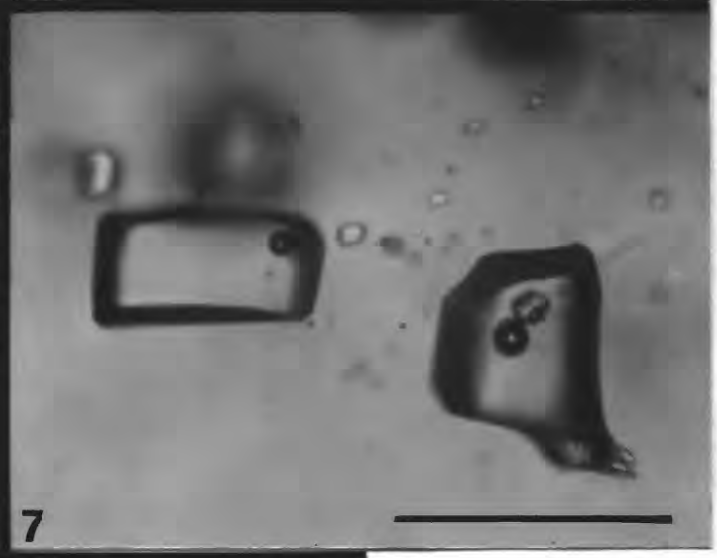
7

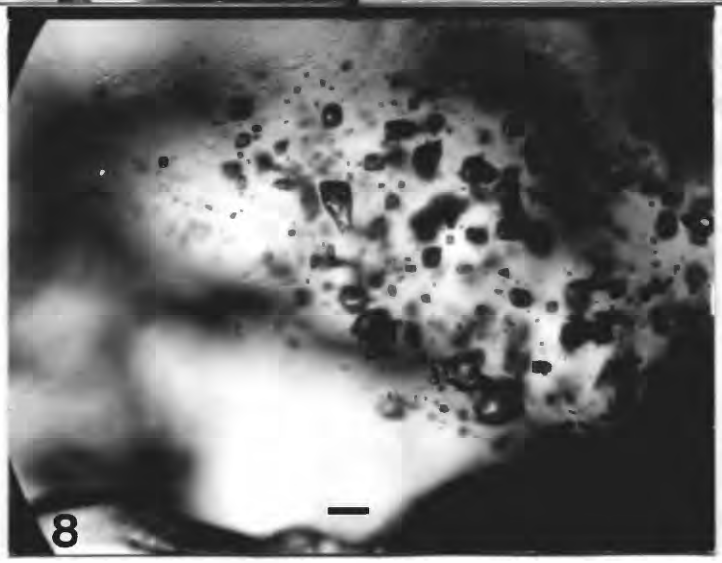
8

Fig. 9 Twin crystal of unidentified birefringent evaporite mineral, completely embedded in a halite crystal, photographed between partly crossed polars, showing many tiny dark inclusions on the interface. The dark specks out in the host salt are mainly artifacts. Sample 24R. Scale bar 100 μm.

Fig. 10 Small birefringent crystal embedded in salt crystal and coated with tiny gas(?) inclusions. Sample 41R. Scale bar 100 μm.

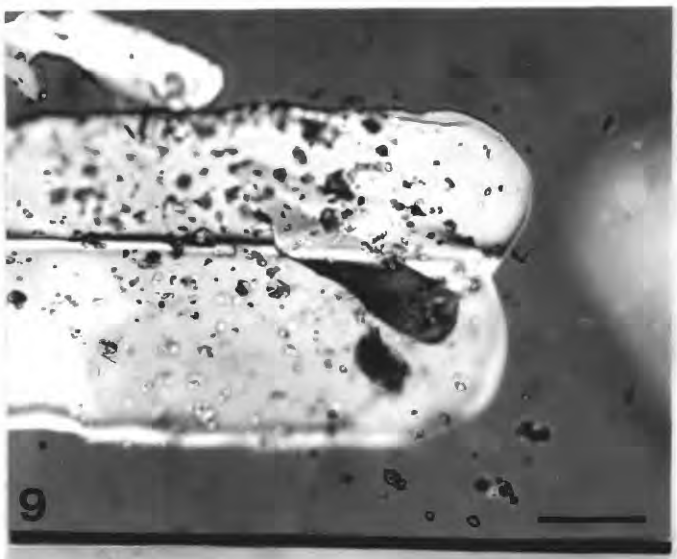
9

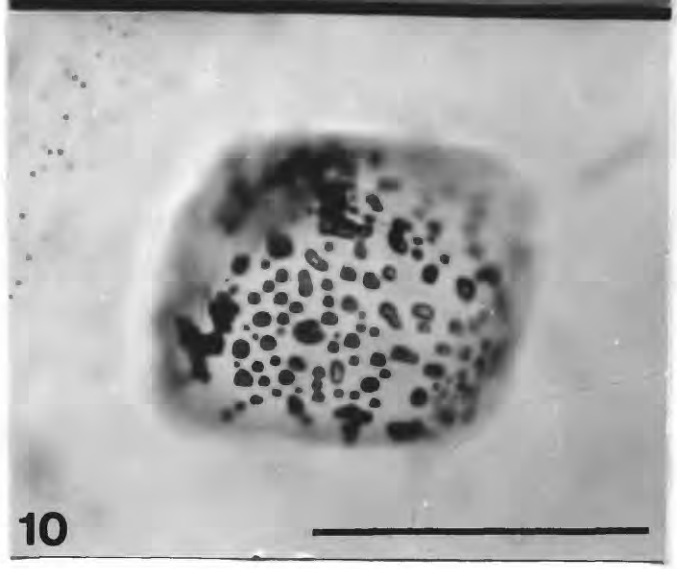
10

Fig. 11 Inclusion-rich grain in sharp contact with other inclusion-free grains, in sample 17R. Scale bar 1 mm.

Fig. 12 Inclusion-rich single crystal of salt from sample 14R. This is a cleavage fragment; the nearly horizontal curving dark lines at the lower left are surface cleavage steps. The small inclusions mostly lie on a series of otherwise invisible three-dimensional "walls", outlining inclusion-free salt "cells." Scale bar 1 mm.

Fig. 13 Close-up of part of a single inclusion-rich salt crystal in Fig. 11, showing a network of many small inclusions with clear salt between. One much larger inclusion is seen to the right. Scale bar 1 mm.

Fig. 14 Detail of inclusions shown in Fig. 11. Central inclusion is essentally a wet mass of unidentified, highly birefringent crystals; inclusion at right has more liquid and hence is subspherical. Numerous small birefringent blades occur as a halo around the larger inclusions. Each of these blades has lens-shaped blebs of liquid on each side. Scale bar 100 μm.

Fig. 15 Semiglobular, crystal-rich inclusion in inclusion-rich grain shown in Fig. 13. Scale bar 100 μm.

Fig. 16 Negative crystal inclusions of brine with a few solid crystal inclusions from sample 14R. Scale bar 10 μm.

Fig. 17 Similar inclusion from sample 35R. Scale bar 100 μm.

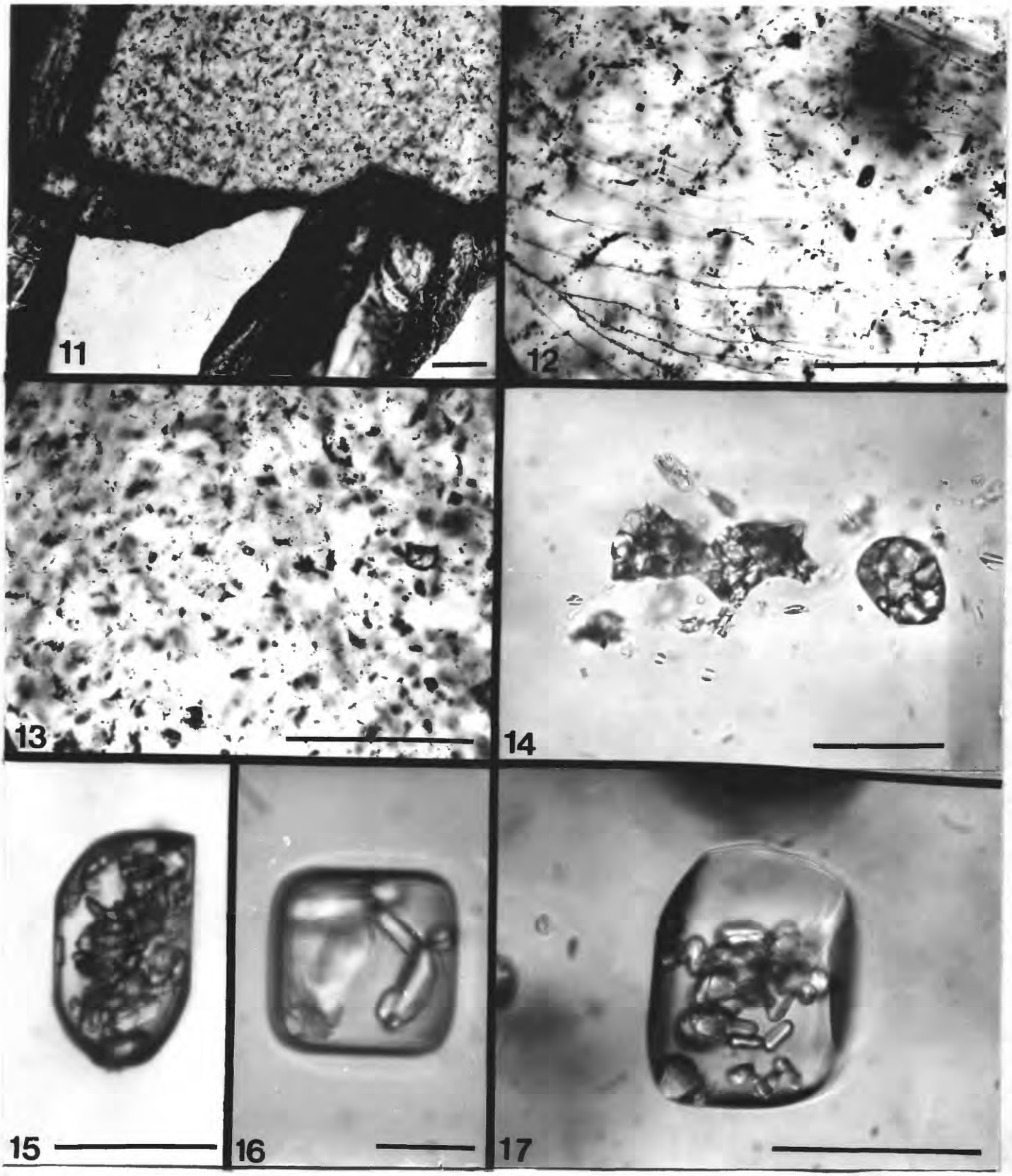
11
12
13
14
15
16
17

Fig. 18 Large, flat, gas bubbles in secondary inclusions (arrows) at edge of core sample 27R, presumably formed when the brine lubricant used in sample preparation entered a fracture formed during the coring and became trapped by recrystallization. Scale bar 100 μm.

Figs. 19 and 20 Plane of secondary inclusions (parallel to 110) in salt of sample 14R. One of the inclusions in the center of the field of Fig. 19 is enlarged in Fig. 20 to show a globule of petroleum (?) plus a solid crystal. Scale bar in Fig. 19 100 μm; in Fig. 20 10 μm.

Figs. 21-23 Planes of secondary intracrystalline inclusions on fractures within single salt crystals, from sample 11R (Figs 21&22) and 14R (Fig. 23). The darker parts of inclusions in Fig. 21 are gas (G), and the light parts are liquid (L). In Fig. 22, the gas bubbles (G) have somewhat darker outlines. This crack wedges off to nothing at the right side. The inclusions in Fig. 23 may be either all gas or all liquid (presumably the latter). Scale bar 100 μm.

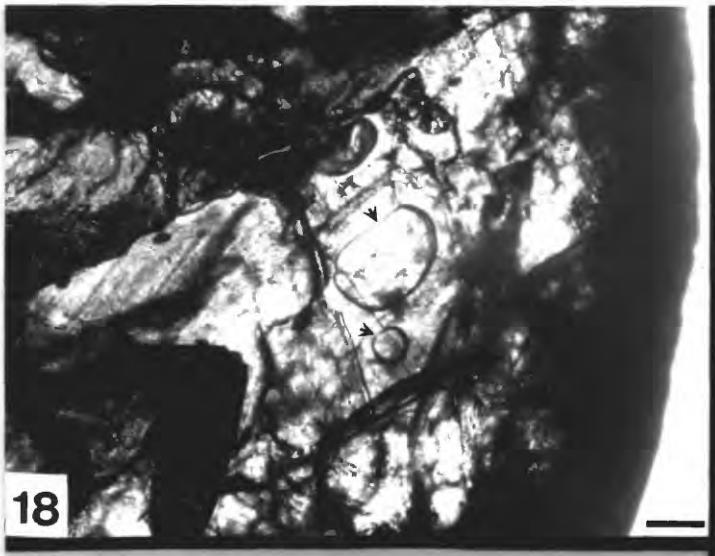
18

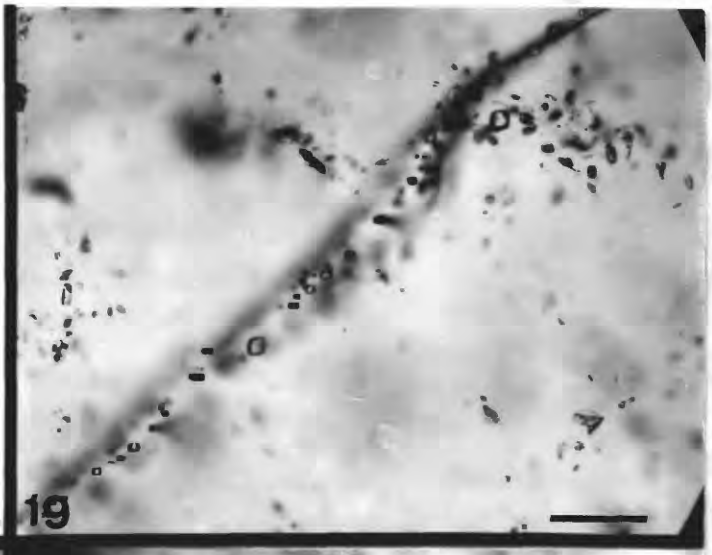
19

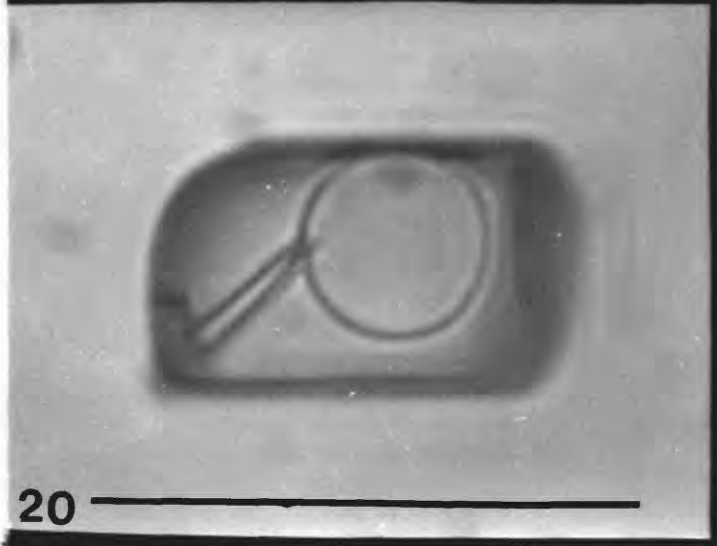
20


G
L
21

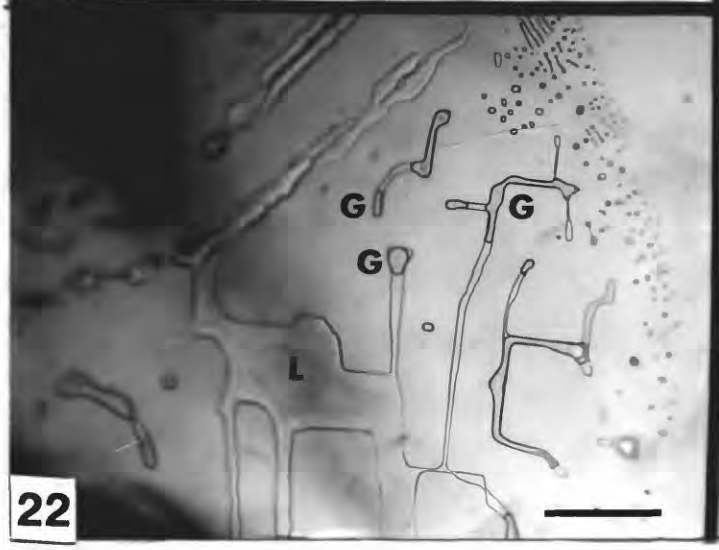
G
G
G
L
22

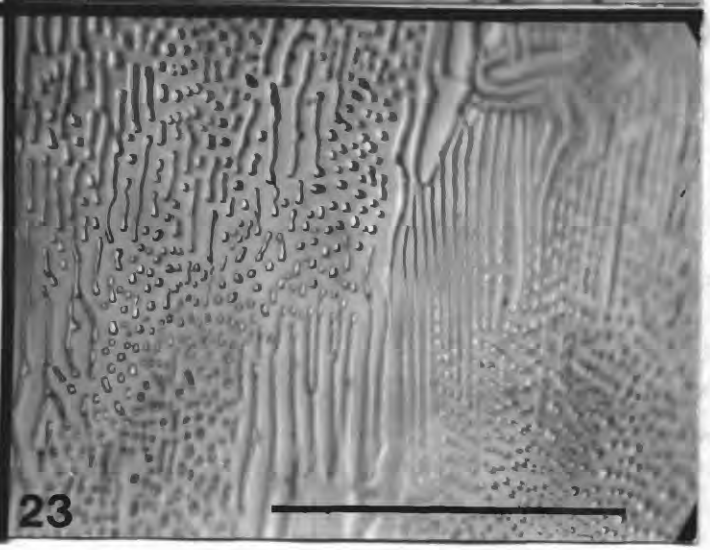
23

Figs. 24-26 Three photographs of the same area in sample 8R, showing three salt grains, A,B, & C, in contact. Fig. 24 is taken in transmitted light; Figs. 25 and 26 are taken in reflected light. The bright spots in Figs. 25 and 26 are subsurface reflections from irregularities in the sloping grain boundaries. See text for explanation. Scale bar 1 mm.

Figs. 27-29 Three photographs of the same area in another part of sample 8R in transmitted light (Fig. 27) and in reflected light (Figs. 28 & 29). See text for explanation. Scale bar 1 mm.

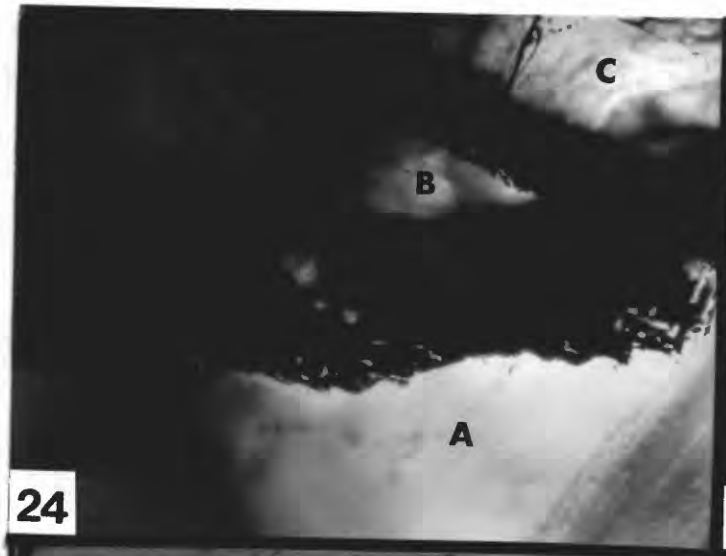
C
B
A
24


27

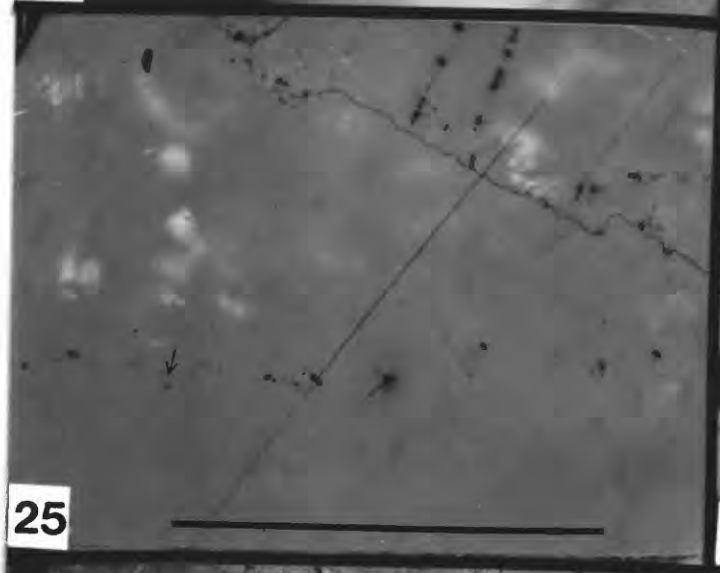
25

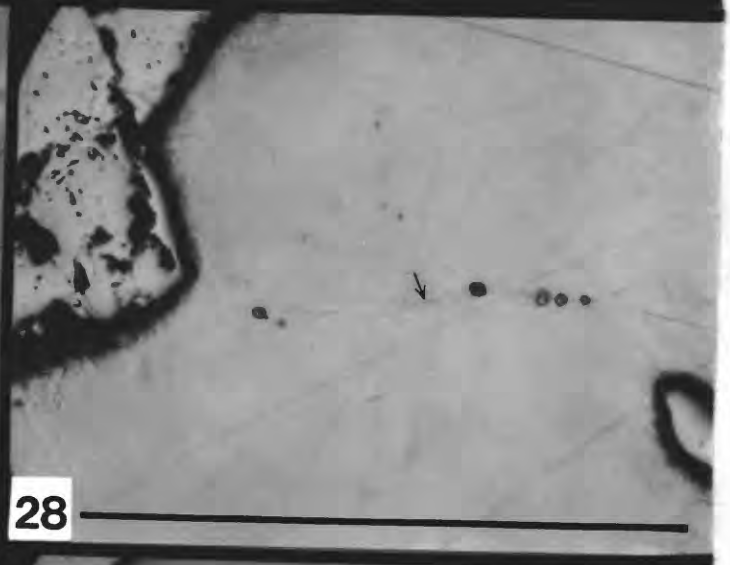
28


26


29

Fig. 30 Grain boundary in sample 8R in reflected light, that is decorated with both inclusions and accessory mineral grains. Hairline cracks are present on almost all interfaces. Scale bar 100 μm.

Fig. 31 An approximately 120° grain intersection in sample 8R, viewed in reflected light. Note that the grain boundaries are hairline cracks, but are complexly crenulated. Scale bar 100 μm.

Fig. 32 Inclusion-rich area in sample 35R that is crossed by a fracture that extends in from the lower left as far as the dotted line. Four large liquid inclusions (arrows) have been partly to completely emptied. The group of four inclusions in the lower right are enlarged in Fig. 33. Scale bar 100 μm.

Fig. 33 Enlarged view of the four large liquid inclusions in lower right of Fig. 32. The innermost edge of the fracture plane (now a secondary plane of liquid and vapor inclusions) is marked by a dotted line; this plane did not reach the two inclusions in the upper right. (These two are at a slightly different plane of focus and hence had to be photographed separately.) Scale bar 100 μm.

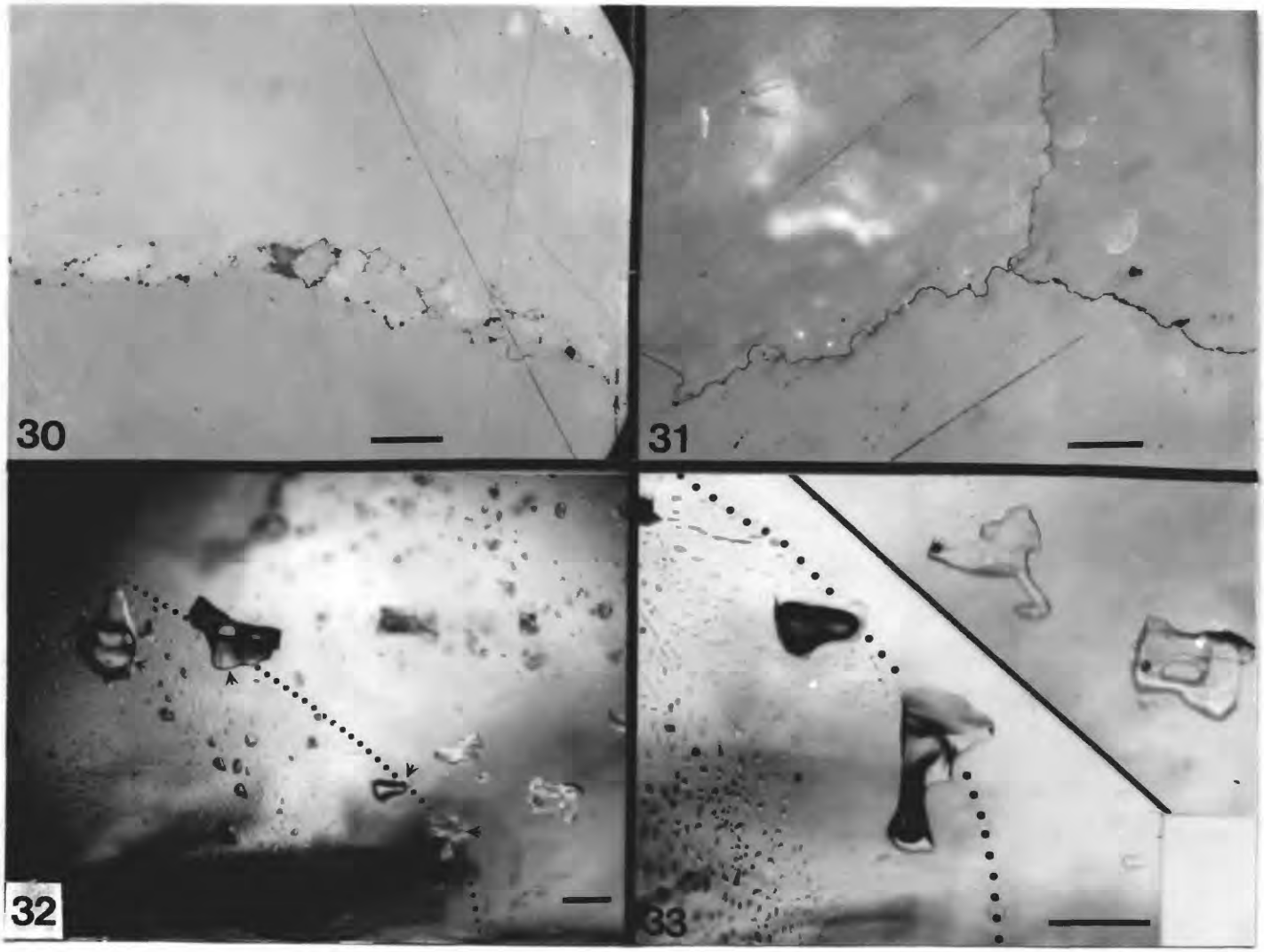
30
31
32
33

Fig. 34 Inclusions of high-pressure gas at interface between birefringent crystal and embedding single salt crystal, in sample 20R, during release by an advancing solution front (coming down from above). Fig. 34 left, shows the grain before solution. In Fig. 34 center, the solution front has released one small bubble, and Fig. 34 right, taken shortly after 34 center, several large bubbles have been evolved. Scale bar 100 μm.

Fig. 35 Another pair of crystals, similar to Fig. 34, in same sample. Note that large gas bubbles are evolved (Fig. 35 right) even though no obvious gas inclusions were present before solution (Fig. 35 left). Scale bar 100 μm.

Fig. 36 Intergranular plane of mainly single phase inclusions in sample 14R that are seen to be filled with gas under pressure during water solution. Scale bar 100 μm.

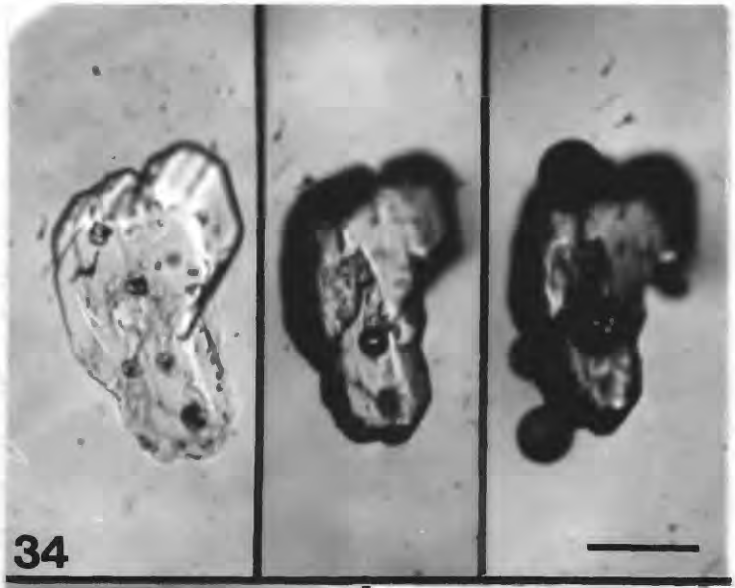
34

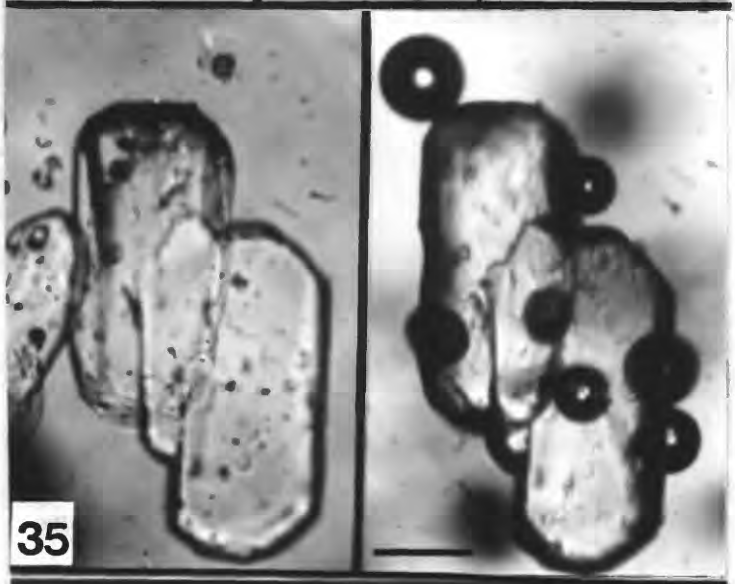
35

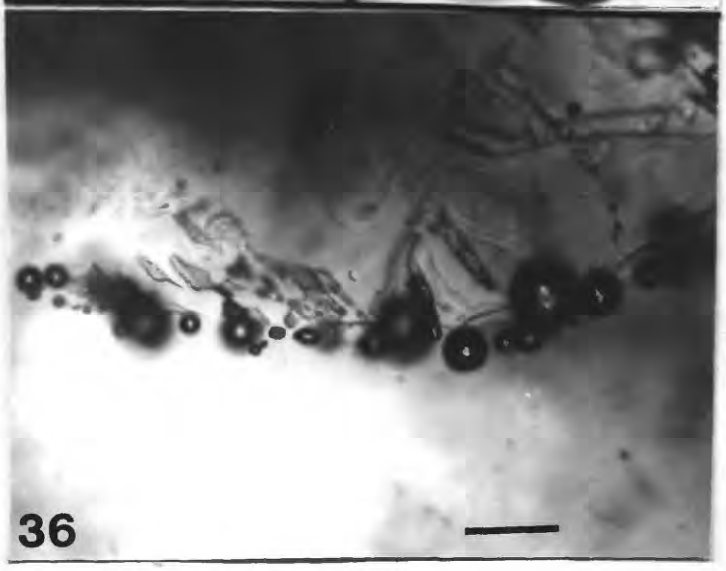
36